
LOCALFORMER: A LOCALITY-PRESERVING VISION TRANSFORMER

A PREPRINT

Qingsong Zhao

Tongji University, China

qingsongzhao@tongji.edu.cn

Zhipeng Zhou

Chinese Academay of Sciences, Beijing, China

zhouzhipeng113@mails.ucas.ac.cn

Yi Wang

Shanghai AI Laboratory, China

wangyi@pjlab.org.cn

Yu Qiao

Shanghai AI Laboratory, China

qiaoyu@pjlab.org.cn

Cairong Zhao 

Tongji University, China

zhaocairong@tongji.edu.cn

April 25, 2023

ABSTRACT

Zigzag flattening (ZF) is commonly used in computer vision as a default option to unfold matrices, *e.g.*, in patch slicing for Vision Transformer (ViT). However, when decomposing multi-scale-object web images, ZF cannot preserve the smoothness of local information well. To address this, we draw inspiration from Space-Filling Curves (SFC) and investigate Hilbert flattening (HF) as an alternative for visual models. We provide a comprehensive theoretical discussion and practical analysis, demonstrating the superiority of HF over other SFC in locality and multi-scale robustness. We leverage HF to alleviate the problem of the lack of locality bias in the shallow layers of ViT, which formulates our Localformer. Extensive experiments demonstrate that Localformer consistently improves performance for several common visual tasks. Additionally, upon inspection, we find that Localformer enhances representation learning and length extrapolation abilities of ViT.

1 Introduction

Humans typically read text in rows and columns, but when it comes to images, we tend to focus on areas of greatest interest first before looking at the other areas. In contrast, computers read both text and images as text. Text is like a one-dimensional timeline, while images are like static real-world scenes projected onto a two-dimensional screen. The key information in an image can be seen as an undirected graphBronstein et al. [2021], and it cannot be represented in a one-way vector without losing important details. This is illustrated in Fig. 1 (a) and (b), which show that the meaning conveyed by the image remains the same after rotation. However, the key information in a text must remain fixed, as any change in position would alter the original message. To accurately encode text, the Transformer Vaswani et al. [2017] model uses a position encoding module to capture the sequence order. In contrast, the key information in an image, consisting of a whole patch, would remain unchanged even after panning or scaling, as shown in Fig. 1 (a) and (c). However, moving the feature points within a semantic patch would significantly alter the meaning conveyed by the image, as shown in Fig. 1 (a) and (d). In summary, there are fundamental differences in the way text and images represent information. Hence, it is naive to apply the mode of reading text directly for the common flattening operation in computer vision.

In deep learning, we often need to extract semantics from input feature maps or tokens. To do this, we typically flatten these high-dimensional tensors into a high-level representation vector, disregarding their local smoothness. Although flattened results tend to ignore the locality descriptions, specific flatten approaches still retain some of these details. For example, the commonly used Zigzag method preserves the spatially neighboring (1 pixel away) key points in their original 2D arrangement, except for the turning points in the Zigzag unfolding. However, as the feature map's scale increases, the flattened 1D vectors' local smoothness becomes more distorted.

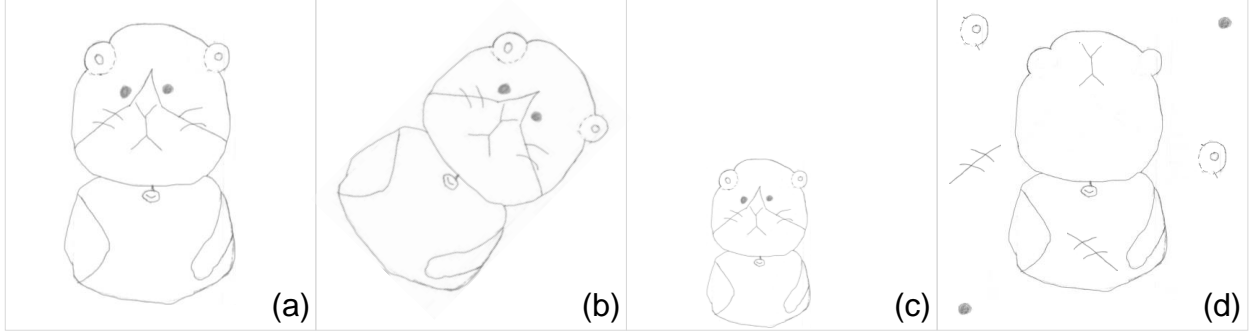


Figure 1: Illustration of Image Reading.

The locality bias, also known as locality or local smoothness, is a widely accepted hypothesis in visual tasks. It suggests that adjacent pixels are more likely to belong to the same object than distant pixels Pathak et al. [2016], Zhang et al. [2014]. Convolutional neural networks (CNNs) have been critical to the success of deep learning in computer vision, primarily due to the strong inductive bias towards local shift-equivariance encoded by the convolution operator. This is essential for learning generic visual representations Nguyen et al. [2020], Sun et al. [2022]. However, more recently, convolution-free architectures such as Vision Transformers (ViT) have become the model of choice. ViT slices the image and treats it as a fixed length of 16×16 words, using multiple self-attention operators to obtain the aggregation of global information. While ViT incorporates more global information than CNNs at lower layers with a uniform representation structure, it is not effective at incorporating local information at lower layers. This is crucial to the ViT model for a strong performance from scratch at scale. Previous studies Nguyen et al. [2020], Steiner et al. [2021] have claimed that large-scale pre-training data could help shallow self-attention layers learn to incorporate this local information. However, not all researchers have access to or can use large image datasets (e.g., JFT-300M Sun et al. [2017]) for training.

Several researchers have explored ways to improve the ability of Vision Transformer (ViT) to capture local information in images. Some of these researchers Wang et al. [2021], Liu et al. [2021a], Li et al. [2022], Zhang and Zhang [2022], Zhang et al. [2021a] drew inspiration from the local sliding window structure in Convolutional Neural Networks (CNNs) and suggest that the shift-equivariant of convolution can enhance ViT's ability to capture local information. Others Yuan et al. [2021], Hassani et al. [2022], Bolya et al. [2022], Renggli et al. [2022] focused on patch aggregation modules to connect semantically similar patches and merge them, thereby improving ViT's training efficiency on small datasets like ImageNet-1K Russakovsky et al. [2015], while also enhancing its performance. In contrast, our approach draws inspiration from the field of geometric fractals to maintain stable locality preservation when slicing patches. We believe that the excellent properties of space-filling curves can help vanilla ViT incorporate more local information, which could bring a paradigm shift in research. Our approach also outlines the significance of 1D operators like fully connected layers and depth-wise separable convolutions, as they can flatten input signals of any form into a vector for processing.

Our investigation shows that the Hilbert curve outperforms other space-filling curves in preserving spatial locality during multi-scale transformations of dimensional space in Mathematics Moon et al. [2001]. In this paper, we provide a detailed analysis of its theoretical guarantees for locality preservation and multi-scale robustness in computer vision compared to other flattening curves. We then propose a new improved Vision Transformer called Localformer by integrating the advantages of Hilbert flattening into the vanilla ViT model, and demonstrate its effectiveness in various vision tasks. Additionally, we examine the internal representation of the Localformer to interpret experimental phenomena. Our contributions are summarized as follows:

- Given theoretical discussion and experimental analysis of local smoothness, we advocate using Hilbert flattening to replace the default Zigzag flattening operation in the vision community.
- We propose a new visual backbone, Localformer, which introduces Hilbert token sampling and a token aggregator into the Vision Transformer architecture to enhance its locality-preserving ability.
- We conduct numerous experiments on image classification and semantic segmentation tasks, and the results show that Localformer consistently outperforms baselines. Furthermore, we reveal a surprising connection between the representation structure and patch flattening operation in Vision Transformers.

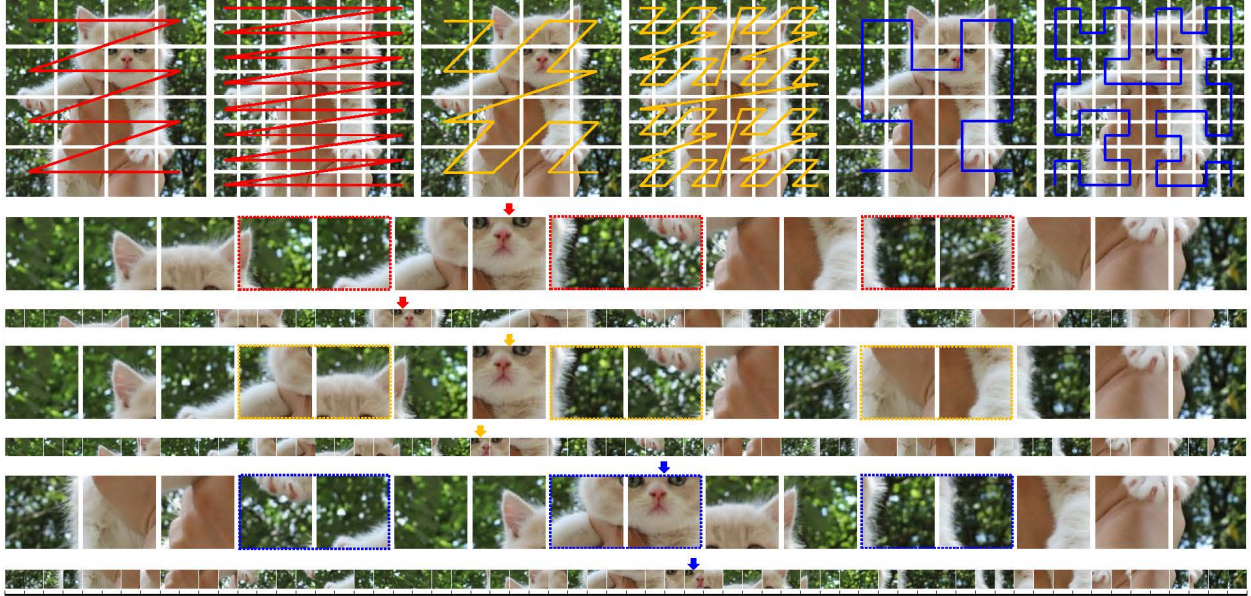


Figure 2: Different flattening methods for image patch unfolding. The first row shows the three flattening curves schematically, in which, the red lines indicate the default Zigzag curve, the yellow lines show the Morton curve (aka Z-order or Lebesgue curve Lebesgue [2003]), and the blue lines show the Hilbert curve. The remaining rows correspond to the visualization of the above three curves in turn. When flattening a 2D image into a 1D patch sequence, the Zigzag and Morton curves will move the initially adjacent image patches (semantically related patches) away from each other, but the Hilbert curve does not. That is, the head of the cat remained clustered together after slicing at different patch scales.

2 Related Works and Preliminaries

2.1 Hilbert Curve Applications

Such prominent works in Mathematics as Jagadish [1990], Gotsman and Lindenbaum [1996], Moon et al. [2001] have evidenced that the locality between objects in multi-dimensional space is preserved in linear space. Inspired by this idea, recent works consisting of Tsinganos et al. [2019], Bappy et al. [2019], Zhang et al. [2021b] have been proposed to introduce the Hilbert curves into a computer vision (CV) application. Bappy et al. [2019] claim that the order of the pixel has a significant impact on the performance of the Long-Short Term Memory (LSTM), and if the Zigzag flattening was performed in the horizontal direction, the neighboring pixel in the vertical direction is far apart. So they utilized the Hilbert curves to arrange pixels before they were fed into the LSTM model. Similarly, to extract better spatial features, FDPT Zhang et al. [2021b] also utilized the Hilbert curves to flatten image pixels before feeding them into the Gated Recurrent Unit (GRU). By contrast, Tsinganos et al. [2019] employ the Hilbert curves to generate 2D image representations from 1D surface electromyography (sEMG) signals, then the features of the sEMG signals were extracted by the CNNs backbones. These above methods only apply the Hilbert curve to a specific CV task without theoretical analysis and empirical proof.

2.2 ViTs and MLPs

Vision Transformer Dosovitskiy et al. [2021] inspires a new paradigm architecture that differs from CNNs by utilizing patch embedding instead of taking images directly as input. Swin Transformer Liu et al. [2021b] proposes shifted windows to solve larger variations of the input image caused by the multi-scale and high resolution. By contrast, MLP-Mixer Tolstikhin et al. [2021] proposed a new architecture that differs from CNNs and Transformers by eliminating the need for convolution and self-attention, and relies only on the repeated implementations of multi-layer perceptron across the spatial or feature channels. Those works all employed Zigzag flattening to expand 2D images or features into 1D patch or token sequences. This paper explores the space-filling curves whose cluster properties outperform Zigzag for those architectures.

2.3 Length Extrapolation

The length extrapolation is a significant challenge for Transformer models, leading to inconsistencies between training and predicted lengths Press et al. [2021], Kiyono et al. [2021]. This challenge is particularly relevant in visual tasks, where good length extrapolation can improve performance. Inconsistencies may arise from two factors: 1) the use of an untrained position embedding weight in predictions, and 2) the number of tokens processed by the attention mechanism at prediction far exceeds the number at training. In fact, the Transformer with relative position encoding has cleverly solved the above two problems and become a strong baseline model. And the current works Su et al. [2021], Chi et al. [2022] can be seen as its variants. Although some researches Zhang et al. [2021a], Liu et al. [2021a] demonstrate the relative positional encoding outperforms absolute positional encoding in image classification task, recent work Wu et al. [2021] claims that the relative positional encoding can not work equally well as the absolute positional encoding in dense prediction visual tasks (e.g., semantic segmentation). Unlike the above works, this paper aims to enhance the length extrapolation capability of absolute position encoding. To the best of our knowledge, we are the first to introduce the space-filling curves into the Vision Transformer to enhance its length extrapolation.

2.4 Preliminaries

We start this section with an introduction to the Space-Filling curves, then give the definitions of Hilbert curve and Morton curve. The definitions and known theorems used in this paper mainly come from Sagan [2012], please refer to it for more details.

Space-Filling Curves A continuous curve is called *space-filling curve* if it can pass through every point of a closed square Peano [1890]. More precisely, a space-filling curve Simmons [1963] is a continuous mapping from a closed unit interval $I = [0, 1]$ to a closed unit square $[0, 1] \times [0, 1]$. The formal definition of space-filling curve is shown as follows:

Definition 2.1 A mapping $f: I \rightarrow E^n (n \geq 2)$ is continuous and $f(I)$ has positive Peano–Jordan measure, then $f(I)$ is called a space-filling curve, where E^n denotes an n -dimensional Euclidean space.

Hilbert Curve Hilbert [1935] is the first generic geometric program that allows the construction of entire classes of space-filling curves. Compared to Zigzag curves and Morton curves, Hilbert curves were the best at minimizing the number of clusters Jagadish [1990]. We denote \mathcal{I} and \mathcal{Q} as the interval $[0, 1]$ and square $[0, 1] \times [0, 1]$ respectively. The generating process of Hilbert curve is driven by the following:

$$\begin{aligned} \mathcal{H} : t \in [0, 1] &\mapsto \mathcal{H}(t) \in [0, 1] \times [0, 1], \\ t = 0.q_1q_2 \dots, 0 \leq q_j &\leq 3, \\ \mathcal{H}(t) = \left(\begin{array}{c} \mathcal{R}e \\ \mathcal{I}m, \end{array} \right) \lim_{n \rightarrow \infty} T_{q_1} T_{q_2} \dots T_{q_n} \mathcal{Q}, \end{aligned} \tag{1}$$

where t is represented in quaternary form. The definition of $\{T_i | 0 \leq i \leq 3\}$ is defined as follows:

$$\begin{aligned} T_i z &= \frac{1}{2} H_i z + h_i, 0 \leq i \leq 3, \\ H_0 z &= \bar{z}i, H_1 z = z, H_2 z = z, H_3 z = -\bar{z}i, \\ h_0 &= 0, h_1 = \frac{i}{2}, h_2 = \frac{1+i}{2}, h_3 = \frac{2+i}{2}, \end{aligned} \tag{2}$$

where we consider complex numbers $z \in \mathbb{C}$ as $(Re(z), Im(z)) \in \mathcal{Q}$. The transformations $\{T_i | 0 \leq i \leq 3\}$ defined above correspond to different geometric deformations. Take transformation T_0 as an example, we first shrink the original \mathcal{Q} towards the original point under the ratio $\frac{1}{2}$, then reflect on the imaginary axis by multiplying with -1 and rotate the square through 90° by multiplying with imaginary number i .

During the generating process of Hilbert curve, the sub-squares shrink into points, which claims that $\mathcal{H}(t)$ is a point in \mathbb{R}^2 . we construct the n -th approximation of Hilbert curve by n -th iteration, which is denoted as \mathcal{H}_n ,

$$\begin{aligned}
 \mathcal{H}_n(0.q_1q_2 \cdots q_n) &= \binom{\mathcal{R}e}{\mathcal{I}m} \sum_{j=1}^n \frac{1}{2^j} H_{q_0} H_{q_1} H_{q_2} \cdots H_{q_{j-1}} h_{q_j}, \\
 &= \sum_{j=1}^n \frac{1}{2^j} (-1)^{e_{0j}} \operatorname{sgn}(q_j) \binom{(1-d_j)q_j - 1}{1 - d_j q_j} \\
 \operatorname{sgn}(x) &= \begin{cases} 1, & \text{if } x > 0, \\ 0, & x = 0. \end{cases} \\
 e_{kj} &= \#(\text{"k" preceding } q_j) \mod 2, \\
 d_j &= e_{0j} + e_{3j} \mod 2,
 \end{aligned} \tag{3}$$

where $\#$ is the counting function and $k \in \{0, 3\}$. We have drawn the image points of finite quaternary ($2 \leq n \leq 3$) connected by straight lines in Figure 2 left. And, note that the order n approximation of Hilbert curve originates in the lower-left sub-square and terminates in the lower-right sub-square. The exit point from each sub-square coincides with the point which goes into the following sub-square.

Morton Curve The generating process of Morton curve is similar to Hilbert curve's. We first denote the n -th approximation of Morton curve as \mathcal{M}_n . Morton curve is the limit of \mathcal{M}_n as n goes to infinity. The conversion function from binary to decimal is denoted by \mathcal{B} . The generating process of Morton curve is driven as follows:

$$\begin{aligned}
 \mathcal{M}_n : t \in \mathcal{I} &\mapsto \mathcal{M}_n(t) \in \mathcal{Q} \\
 \mathcal{M}_n\left(\frac{\mathcal{B}(q_1q_2 \cdots q_n)}{2^n - 1}\right) &= \left(\begin{array}{c} \frac{\mathcal{B}(q_1q_3 \cdots q_n)}{2^{n/2}} \\ \hline \frac{\mathcal{B}(q_2q_4 \cdots q_{n-1})}{2^{n/2}} \end{array} \right) \triangleq p \in \mathcal{Q} \\
 \mathcal{M}_n(t) &= p_0 * (1 - s) + p_1 * s, t \in [\mathcal{M}_n^{-1}(p_0), \mathcal{M}_n^{-1}(p_1)] \\
 \text{where } s &= \frac{t - \mathcal{M}_n^{-1}(p_0)}{\mathcal{M}_n^{-1}(p_1) - \mathcal{M}_n^{-1}(p_0)} \in [0, 1], q_i \in \{0, 1\}
 \end{aligned} \tag{4}$$

3 Flattening

In performing the tensor flattening operation, computers may benefit from the researcher's intuitive reading of text. This inadvertent action resulted in the widespread use of Zigzag flattening as a standard tensor operation in computer vision. The inspiration for this method came from the elegant space-filling curves in mathematics, which possess desirable qualities for preserving locality when flattening multi-dimensional feature maps into a 1D vector. Additionally, these curves maintain locality preservation when scaling up or down the target feature maps. This section introduces three flattening methods, followed by a theoretical discussion on the definitions of locality preservation and general equivariance. Finally, we present a practical analysis of two toy applications in visual tasks.

Zigzag Flattening We study the ZF operation on image with size of $H \times W$. For convenience, we can assume that both H and W are equal to 1 and divided uniformly into 2^n parts. Given a real number $t \in [0, 1]$ which can be represented in quaternary form with finite length: $t = 0.q_1q_2 \cdots q_n$, the ZF is defined by \mathcal{Z}^{-1} as follows:

$$\mathcal{Z} : 0.q_1q_2 \cdots q_n \mapsto \left(\begin{array}{c} \left(\sum_{k=1}^n q_k 4^{n-k} \% 2^n \right) * \frac{1}{2^n} + \frac{1}{2^{n+1}} \\ \hline \left(\sum_{k=1}^n q_k 4^{n-k} \right) \% \left(\frac{2^n}{2} \right) * \frac{1}{2^n} + \frac{1}{2^{n+1}} \end{array} \right) \tag{5}$$

$$\mathcal{Z}^{-1} : \left[\frac{i}{2^n}, \frac{j}{2^n} \right] \mapsto 0.q_1q_2 \cdots q_n = \mathcal{Z}^{-1}\left(\left[\frac{i}{2^n}, \frac{j}{2^n} \right]\right), \tag{6}$$

where $0 \leq i, j \leq 2^n - 1$.

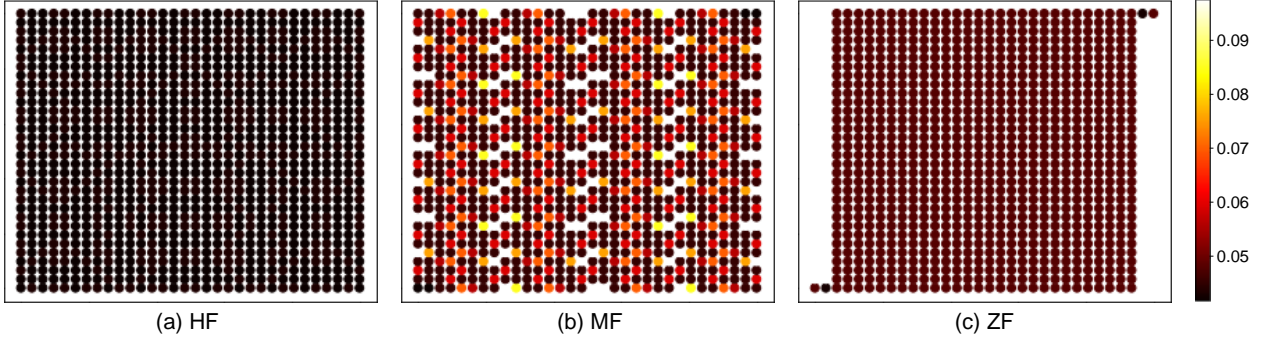


Figure 3: The heat maps of MAD with $K = 2$, the brightness of the pixels indicates the 2D position information preservation. The closer the pixels are to black, the better.

Table 1: The percentage of points with MAD is smaller than the given MAD threshold ϵ , where we set $K = 2$. Indexing pixel points within the same 2D neighborhood, the larger the percentage indicates the better position information preservation.

ϵ	0.043	0.045	0.047	0.053	0.055	0.057	0.059	0.069	0.070	0.071	0.077	0.086	0.087	0.120
HF	60.16%	100.00%	100.00%	100.00%	100.00%	100.00%	100.00%	100.00%	100.00%	100.00%	100.00%	100.00%	100.00%	100.00%
MF	0.39%	0.39%	62.89%	62.89%	62.89%	69.14%	69.14%	81.64%	81.64%	87.89%	91.02%	91.02%	92.58%	92.58%
ZF	0.00%	0.20%	0.20%	87.89%	87.89%	87.89%	87.89%	87.89%	87.89%	87.89%	87.89%	87.89%	87.89%	87.89%

Morton Flattening According to the definition of Morton Curve in Equation (4), we define the Morton Flattening of order n by

$$\mathcal{M}_n^{-1} : \begin{pmatrix} \frac{\mathcal{B}(q_1^0 q_2^0 \cdots q_{n-1}^0)}{2^{n/2}} \\ \frac{\mathcal{B}(q_1^1 q_2^1 \cdots q_{n-1}^1)}{2^{n/2}} \end{pmatrix} \mapsto \frac{\mathcal{B}(q_1^0 q_1^1 \cdots q_{n-1}^0 q_{n-1}^1)}{2^n - 1} \quad (7)$$

where \mathcal{M}_n^{-1} is the inverse mapping of \mathcal{M}_n .

Hilbert Flattening Hilbert flattening is built upon the Hilbert curve, with the approximation of Hilbert curve of order n , we can define the operation Hilbert Flattening. Consider an image with resolution $n \times n$, the inverse map of approximation of Hilbert curve of order n provides the mechanism of Hilbert Flattening of order n :

$$\mathcal{H}_n^{-1} : \begin{pmatrix} \frac{i}{2^n} + \frac{1}{2^{n+1}} \\ \frac{j}{2^n} + \frac{1}{2^{n+1}} \end{pmatrix} \mapsto = 0.q_1 q_2 \cdots q_n, \quad (8)$$

where $\mathcal{H}_n(0.q_1 q_2 \cdots q_n) = (\frac{i}{2^n} + \frac{1}{2^{n+1}}, \frac{j}{2^n} + \frac{1}{2^{n+1}})^T$. Then the pixel on the image contains point $(\frac{i}{2^n} + \frac{1}{2^{n+1}}, \frac{j}{2^n} + \frac{1}{2^{n+1}})^T$ will be assigned the value $0.q_1 q_2 \cdots q_n$. All the pixels on the images will be ordered by their values, which in fact gives the definition of Hilbert Flattening.

3.1 Theoretical Discussion

In this subsection, we provide a theoretical and qualitative discussion of the above flattening operations, including Zigzag flattening, Hilbert flattening, and Morton flattening.

Evaluate Locality Preservation Mathematically How to evaluate the locality preservation of the flattening operation mathematically? We introduce a definition of the limit, the dilation factor. Specifically, given two points $t_1, t_2 \in [0, 1]$, the quaternary form are represented as $t^1 = 0.q_1^1 q_2^1 \cdots$ and $t^2 = 0.q_1^2 q_2^2 \cdots$ when these two points are close. It means that for an large integer j such that $q_k^1 = q_k^2, \forall 1 \leq k \leq j$. By applying the formula in Equation 3, we obtain the distance between points of $\mathcal{H}(t^1), \mathcal{H}(t^2)$ as follows:

$$|\mathcal{H}(t^1) - \mathcal{H}(t^2)|^2 \leq \sum_{k=j+1}^{\infty} \frac{8}{2^k} \leq \frac{8}{2^j}. \quad (9)$$

Table 2: The DTW distance for different fractal curves (i.e., Hilbert curve, Morton curve, and Zigzag flattening) on the proposed toy dataset (consisting of multiple scale object and image resolutions). “L32” means Large scale object with a resolution of 32×32 and “S128” means Small scale one with a resolution of 128×128 . Lower is better.

Scale Methods	L32 vs S32			L32 vs L64			L64 vs S64			L64 vs L128			L128 vs S128			L32 vs S128		
	HF	MF	ZF	HF	MF	ZF	HF	MF	ZF	HF	MF	ZF	HF	MF	ZF	HF	MF	ZF
Circle	5.19	5.71	8.61	4.13	4.97	14.32	6.14	7.86	16.28	6.74	7.29	28.71	9.13	10.20	33.31	3.95	4.38	18.52
Square	3.40	4.06	8.14	5.42	5.49	17.16	6.60	7.26	15.53	7.39	7.61	35.47	10.58	12.23	31.03	8.67	7.61	29.67
Triangle	4.61	4.59	9.60	3.63	4.27	16.03	6.93	6.99	18.83	6.06	6.64	31.55	7.99	9.37	38.07	4.30	4.76	10.28

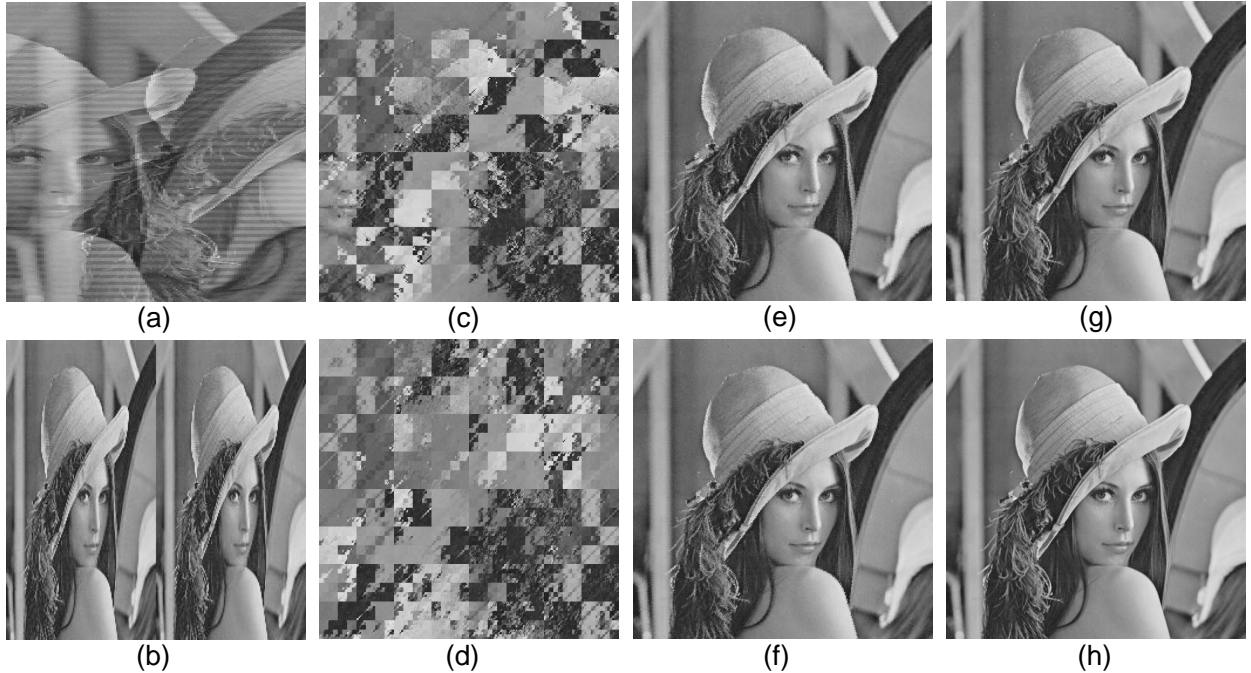


Figure 4: The Lena picture is widely used in the qualitative analysis of digital image processing *e.g.*, Tian [2003]. We report the qualitative results of the 1D interpolation-based image scaling. (a) After expanding the image from 2D to 1D with ZF, we down-sample the original scale 512×512 to 256×256 by the nearest neighbor 1D interpolation algorithm. (b) Again, we do the dimensional transform with ZF first, but up-sample the original scale 256×256 to 512×512 by the same algorithm. (c) Same as (a), but with MF. (d) Same as (b), but with MF. (e) Same as (a), but with HF. (f) Same as (b), but with HF. (g) Original 512×512 Lena. (h) Original 256×256 Lena.

The dilation bound of Hilbert curve is shown in Theorem 3.1, We find that HF operation can obtain a sequence ordering of the image/feature map which guarantees that consecutive parts in sequence are close in the original image. Now we study the dilation factor of the ZF operation on an image with a size of $H \times W$. Let $t^1 = 0.00 \cdots 0 \underbrace{33 \cdots 3}_{\frac{n}{2}}$ and

$t^2 = 0.00 \cdots 0 \underbrace{100 \cdots 0}_{\frac{n}{2}-1 \quad \frac{n}{2}}$, which are consecutive points in the interval $[0, 1]$ with distance $\frac{1}{4^n}$. We have $\frac{|\mathcal{Z}(t^1) - \mathcal{Z}(t^2)|^2}{4^n} = \frac{(1 - \frac{1}{2^n})^2 + \frac{1}{4^n}}{4^n} = 4^n - 2^{n+1} + 2$. Then we get Remark 3.2. And Remark 3.2 has been utilized in the point cloud

classification and segmentation tasks Chen et al. [2022]. For Morton flattening, let $p_0 = \begin{pmatrix} \mathcal{B}(0 \underbrace{1 \cdots 1}_{\frac{n}{2}-1})/2^{n/2} \\ \mathcal{B}(1 \underbrace{\cdots 1}_{\frac{n}{2}})/2^{n/2} \end{pmatrix}$

$p_1 = \begin{pmatrix} \mathcal{B}(\underbrace{10 \cdots 0}_{\frac{n}{2}-1})/2^{n/2} \\ \mathcal{B}(\underbrace{0 \cdots 0}_{\frac{n}{2}})/2^{n/2} \end{pmatrix}$, we have $\mathcal{M}_n^{-1}(p_0) = \frac{2^{n/2}}{2^n-1}$ and $\mathcal{M}_n^{-1}(p_1) = \frac{2^{n/2}-1}{2^n-1}$. So we have

$$\frac{|p_0 - p_1|^2}{|\mathcal{M}_n^{-1}(p_0) - \mathcal{M}_n^{-1}(p_1)|} = \frac{\frac{1}{2^n} + 1}{\frac{1}{2^n-1}} = 2^n - 2^{-n}. \quad (10)$$

Then we get Remark 3.3.

Theorem 3.1 *The square-to-linear dilation factor of the Peano-Hilbert curve is equal to 6 Bauman [2006], which means that the maximum value of $\frac{|\mathcal{H}(t^1) - \mathcal{H}(t^2)|^2}{|t^1 - t^2|} \leq 6$.*

Remark 3.2 *The square-to-linear dilation factor of the ZF curve is ∞ . ($\lim_{n \rightarrow \infty} 4^n - 2^{n+1} + 2 = \infty$).*

Remark 3.3 *The square-to-linear dilation factor of the MF curve is ∞ . ($\lim_{n \rightarrow \infty} 2^n - 2^{-n} = \infty$).*

Evaluate Locality Preservation in Computer Vision How to evaluate the locality preservation of the flattening operation in computer vision? Inspired by the locality assumption in visual tasks, we introduce a definition of locality preservation, Mean Absolute Distance (MAD). Continued above, we draw the conclusion both ZF and MF operations obtain a sequence ordering of the pixel where consecutive points are distant in the original image. Now we explore how much the flattened 1D pixel can preserve the original 2D structure. We first apply those flattening methods respectively to get a sequence of points with fixed length N . For each point p at position i ($1 \leq i \leq N$), we collect the neighbors which are K steps away from p . In order to measure the extent of information preservation, we define the MAD of those pixels with respect to p as follows:

$$\text{MAD}(p) = \frac{\sum_{\substack{i-K \leq k \leq i+K \\ 1 \leq p+k \leq N}} \|\mathcal{F}^{-1}(p_k) - \mathcal{F}^{-1}(p)\|_2}{\#(\text{K step neighbors})}. \quad (11)$$

For clarity, we show the MAD value with a heat map form for all pixels, low is better. Most points have a uniform high MAD value with ZF (i.e., Fig. 3 (c)), and over a certain percentage of points have a small one with MF (i.e., Fig. 3 (b)), while most points have a uniform small MAD value with HF (i.e., Fig. 3 (a)). Moreover, we give the quantitative comparison between the above operations in Table 1 on the percentage of points whose $\text{MAD}^{\frac{1}{2}}$ is smaller than a given threshold ϵ . We also find that the Hilbert flattening has an advantage in the preservation of original locality information over the others.

Evaluate the Stability of Scale Operation How to evaluate the stability of the image scale operation? According to the general equivariant of the convolution operator, we give a corollary about \mathcal{S} -robust of the flattening operator. Take $\Omega = \mathbb{Z}_{2^n} \times \mathbb{Z}_{2^n}$ to be a 2D grid, and $\Omega' = \mathbb{Z}_{2^{2n}}$ to be a 1D sequence, given an RGB image as a mapping: $\Omega \rightarrow \mathbb{R}^3$. As proposed by Bronstein et al. [2021], Wang et al. [2022], the convolutional layers of CNNs are shift-equivariant. The general equivariant is defined as Definitions 3.4 and 3.5. Consider the n -th order and $(n+1)$ -th order approximation of Hilbert flattening as reported in Eq. 3, geometrically, the HF operation just divides the n -th order approximation Hilbert curve uniformly between every pair of endpoints into three parts, then moves the second part away from the original curve with distance $\frac{1}{2^{n+1}}$. Finally, it connects the moving part with the endpoints of the second part. (see Fig. 2 right). Given an image I with size $2^{n+1} \times 2^{n+1}$, we utilize the $(n+1)$ -th order HF to unfold it. We denote the pixel set after flattening as $\mathcal{H}_{n+1}(I)$. Also, we first scale down the image I into image $I_{\frac{1}{2}}$ with size $2^n \times 2^n$. We denote the pixel set after n -th order HF as $\mathcal{H}_n(I_{\frac{1}{2}})$. According to Sec. 3.1 and 3.1, $\mathcal{H}_n(I_{\frac{1}{2}})$ and $\mathcal{H}_{n+1}(I)$ satisfy the following condition:

$$(\mathcal{H}_{n+1}(I))_{\frac{1}{2}} \approx \mathcal{H}_n(I_{\frac{1}{2}}), \quad (12)$$

where $\frac{1}{2}$ means that scaling the image with ratio $\frac{1}{2}$. Consider the scale operation group $\mathcal{S} = \{(\cdot)_{2^{-m}} | m \in \mathbb{Z}\}$, we have

$$(\mathcal{F}_{n+m}(I))_{2^{-m}} \approx \mathcal{F}_n(I_{2^{-m}}), \quad (13)$$

where \mathcal{F} is a flattening operator, and we get the Corollary 3.6. In conclusion, as n approaches a sufficiently large number (i.e., $n \rightarrow +\infty$), we only find the Hilbert flattening is \mathcal{S} -robust.

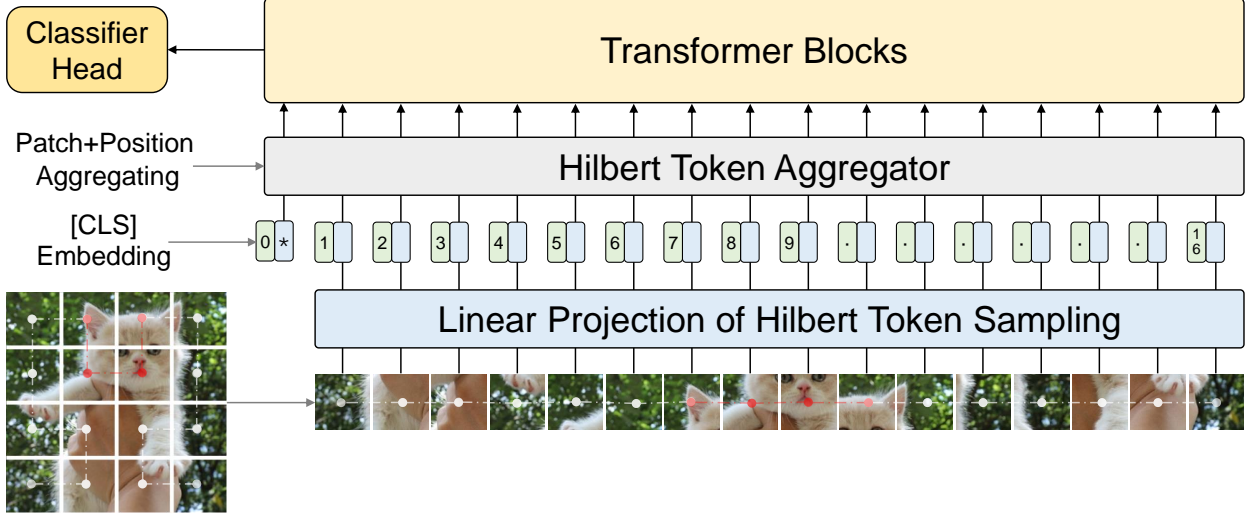


Figure 5: Illustration of our Localformer. The proposed Localformer consists of two critical modules, i.e., Hilbert Token Sampling (HTS) and Hilbert Token Aggregator (HTA). The HTS would not move the initially adjacent image blocks (semantically related patches) away from each other, e.g., the head of cat (red dotted line) remained clustered together after slicing, and the position of it on the sequence would not change. The HTA aggregates the embedded patches to enhance the visual local information similarity.

Definition 3.4 A function $f : \mathcal{X}(\Omega) \rightarrow \mathcal{X}(\Omega)$ is \mathcal{G} -equivariant if $f(\rho(g)x) = \rho(g)f(x)$ for all $g \in \mathcal{G}$, i.e., group action on the input affects the output in the same way, where ρ is a representation of group \mathcal{S} , $\mathcal{X}(\Omega)$ denotes all signals on domain Ω .

Definition 3.5 A function $f : \mathcal{X}(\Omega) \rightarrow \mathcal{X}(\Omega)$ is \mathcal{G} -robust if $f(\rho(g)x) \approx \rho(g)f(x)$ for all $g \in \mathcal{G}$, i.e., group action on the input affects the output in the same way, where ρ is a representation of group \mathcal{S} , $\mathcal{X}(\Omega)$ denotes all signals on domain Ω .

Corollary 3.6 A flattening function $\mathcal{F} : \mathcal{X}(\Omega) \rightarrow \mathcal{X}(\Omega')$ is \mathcal{S} -robust if $\mathcal{F}(\rho(g)x) \approx \rho'(g)\mathcal{F}(x)$ for all $g \in \mathcal{S}$, i.e., group action on the input affects the output in the same way with input and output spaces having different domains Ω, Ω' and representations ρ, ρ' of the same group \mathcal{S} .

3.2 Analysis in Practice

Also, we report two toy experiments that apply the aforementioned three flattening methods to common computer vision operations as shown below.

Image Scaling Image scaling is a common operation in digital image processing (DIP). Two interpolations by row and column respectively are the standard practice for image scaling. But would it work well if we flatten the image and interpolate it only once? As shown in Fig. 4 (a) to (d), with Zigzag flattening and Morton flattening, neither up-sampling nor down-sampling operations result in a normal image. On the contrary, with Hilbert flattening, see Fig. 4 (e) and (f), the good results are obtained regardless of the up-sampling or down-sampling operation. Moreover, the effects of Hilbert scaling can perform favorably against the result of 2D interpolation algorithms.

Dynamic Time Warping Distance Dynamic time warping (DTW) is a prominent approach to obtain an optimal alignment between two given (one-dimension) sequences under certain restrictions Berndt and Clifford [1994], Fang et al. [2020]. Initially, DTW was commonly applied to compare different speech modalities in automatic speech recognition, see Müller [2007]. Here, we produced a toy dataset consisting of three common shapes (circle, square, and triangle), see details in Appendix Fig. 1. All the images are first flattened into a 1D form by three different unfolding strategies (i.e., ZF, MF, and HF, see Fig. 2), then the DTW distance between any two images is calculated as reported in Table 2. When the resolution of picked images is equal, turn up the resolution, and DTW distance between large and small targets will also follow the increase. However, compare to ZF and MF, The DTW value changes of HF are very

small. When the target scale of the two images is equal, turn up the resolution of both, the DTW distance between different resolutions will also follow the increase. HF is still the method with the least variation in DTW values. Also, the DTW value of HF is always the smallest one among all lines, and at the smallest, it is only one-fifth of ZF.

4 Localformer

With the above analysis, we suppose that the space-filling-curve-based flattening operation can be applied to visual tasks. Considering the discussion of Sec. 3, we choose the Hilbert curve as the default space-filling curve for the flattening operation throughout this paper.

4.1 Hilbert Toeken Sampling

In this section, we introduce a new patch flattening operation for the patch embedding block of ViT, namely Hilbert Token Sampling. Tokens extracted from image patches in Vision Transformer are ordered in Zigzag by default. The Hilbert token sampling is an unfolding operation for image patches, unlike the orthodox Zigzag unfolding (Pytorch implementation: `torch.flatten(-)`), which requires image patches to be unfolded in the order of the Hilbert flattening as shown in Fig. 5 bottom left. Our HTS module only replaces the unfolding operation of the original patch embedding and is not a new patch embedding method. Two similar tokens may be far apart after the Zigzag flattening operation, but the distance information between these tokens is vital for some computer vision tasks (*e.g.*, semantic segmentation). From this perspective, we suppose that Hilbert token sampling can alleviate this problem from the root. In addition, the images collected on the web (*e.g.*, ImageNet-1K) do not all conform strictly to the center bias, and the scale of the objects in them varies Li et al. [1994, 2014]. Considering the Hilbert flattening is \mathcal{S} -robust, which \mathcal{S} denotes the scale operation group. We suppose that the proposed HTS can help the original ViT learn a uniform global representational structure, and capture an exact position embedding at a negligible cost.

4.2 Hilbert Token Aggregator

As introduced in Sec. 3.1, the ZF and MF operations will make the adjacent patches to be far away from each other, while the HF not. After our HTS module, it is guaranteed that similar patches are close in the ordered 1D token sequence. This is essential for the proper functioning of the next token aggregator module. For the following self-attention operator to take advantage of this inductive bias (local smoothness). We introduce a generic token aggregator, i.e., Hilbert Token Aggregator, which efficiently enhances the similarity between two adjacent tokens. Specifically, for one input token sequence, the embedding of image patches $\mathcal{X} = \{x_1, x_2, \dots, x_n\}$, where $x_i \in \mathbb{R}^D$, n means the number of patches. And output matrix $\mathcal{X}' = \{x'_1, x'_2, \dots, x'_n\}$, in which each element x'_i is computed by the Eq. 14 as below.

$$x'_i = \mathcal{F}(x_i, k)U_j, \quad (14)$$

where $j \in \{1, 2, \dots, D\}$, $U \in \mathbb{R}^{D \times k}$ is a learnable parameter matrix to integrate the input tokens. And \mathcal{F} is a picking function to generate the neighborhoods of x_i with a radius size k . Then, we obtain the aggregated token embedding $x'_i \in \mathbb{R}^D$ and put them into the next self-attention blocks.

4.3 The Locality-Preserving Vision Transformer

To verify the effectiveness of the above modules, we propose a general-purpose vision backbone named Locality-Preserving Vision Transformer (Localformer), as shown in Fig. 5. Same as vanilla ViT, Localformer applies a universal flat structure that makes feature maps at a single scale. Although the flat structure is not well adapted to the down-stream detection task, it does not under-perform in the pre-train classification task and is more efficient compared to the progressive pyramid structure (*e.g.*, Liu et al. [2021a], Fan et al. [2021]). And the original ViT is still the backbone of choice for the fundamental models (*e.g.*, Radford et al. [2021]). Based on the standard ViT, we only take our Hilbert token sampling module into the shallower patch embedding block, and adopt the proposed Hilbert token aggregator module before the self-attention blocks, while the others remain the same. We also give multiple scale architectures similar to ViT models (*e.g.*, Localformer-B or Localformer-L).

5 Experiments

We begin this section with the effectiveness of our Localformer on image classification and semantic segmentation tasks, and then give a series of inspection studies of the internal representation of Localformer. We utilized the common settings to compare the performance for fairness. With limited computational resources, we are not motivated by

Table 3: Recognition accuracy of different models on ImageNet-1K with multiple settings. “Ave. Pool.” means all tokens are pooled on average as the output of the classifier.

Models	Res.	Ave. Pool.	#Param (M)	Top-1 (%)	Top-5 (%)
ViT-S/16Dosovitskiy et al. [2021]	224 ²	×	22.1	78.10	-
ViT-B/16Dosovitskiy et al. [2021]	224 ²	×	86	79.80	-
ViT-L/16Dosovitskiy et al. [2021]	224 ²	×	304	81.10	-
DeiT-STouvron et al. [2021]	224 ²	×	22.1	79.90	95.00
DeiT-BTouvron et al. [2021]	224 ²	×	86	81.80	95.60
DeiT-BTouvron et al. [2021]	384 ²	×	87	82.90	96.20
T2T-ViT-14Yuan et al. [2021]	224 ²	×	21.5	80.70	-
Swin-TLiu et al. [2021a]	224 ²	✓	28.3	81.30	-
Swin-S3-TChen et al. [2021]	224 ²	✓	28.1	82.10	95.80
ViT-T/16Dosovitskiy et al. [2021]	224 ²	×	5.7	70.38	88.75
ViT-B/16Dosovitskiy et al. [2021]	224 ²	×	86	81.19	95.40
ViT-B/16Dosovitskiy et al. [2021]	224 ²	✓	86	82.02	95.78
ViT-S/14Dosovitskiy et al. [2021]	224 ²	✓	22	80.10	95.19
ViT-L/14Dosovitskiy et al. [2021]	224 ²	✓	304	82.98	96.17
Localformer-T/16	224 ²	×	5.7	70.91	89.22
Localformer-B/16	224 ²	×	86	81.78	95.63
Localformer-B/16	224 ²	✓	86	82.47	96.00
Localformer-S/14	224 ²	✓	22	80.41	95.33
Localformer-L/14	224 ²	✓	304	83.43	96.44

practice-based CV tasks, and we are not good at utilizing tricks at training. Notably, the settings including software (i.e., the virtual environment of Python 3.7 and Torch 1.7.1) and hardware (i.e., 4 NVIDIA A100 GPUs) are strictly consistent. More experimental results, and visualizations can be found in the Appendix.

5.1 Image Classification

We train all models with a fixed input resolution (224×224) on the ImageNet-1K dataset Deng et al. [2009] from scratch. We follow the same settings in DeiT Touvron et al. [2021] by default, which consists of data augmentation, comparison protocols, and regularization. Specifically, we set the drop path rate as 0.1/0.35/0.45 for our small/base/large models. All models are trained 300 epochs with the “AdamW” optimizer and the cosine learning rate schedule, while the first 10 epochs are applied for linear warm-up. The weight decay, learning rate, and batch size are set to 0.05, 1e-3, and 256 respectively.

The results are reported in Table 3, in which all methods employ multi-scale models including tiny, small, base, and large. One can see that the Localformer can improve performance over the ViT (e.g., 0.53% Acc on ViT-T, 0.31% Acc on ViT-S, 0.45% Acc on ViT-B, and 0.45% Acc on ViT-L). Those gains are clear and consistent regardless of model size, which shows the effectiveness and robustness of the proposed Localformer. We also find that the Localformer can bring more gains from ViT if the classifier does not use the average pooling layer (i.e., from 0.45% to 0.59% on ViT-B).

5.2 Semantic Segmentation

Our dense prediction (i.e., semantic segmentation) experiments are conducted on ADE20k dataset Zhou et al. [2017]. We adopt the popular Upernet framework (base on mmseg Contributors [2020] codebase) for fair comparison. We simply apply the settings of the Swin Transformer Liu et al. [2021a] but train the models for 80k iterations. The drop path rates are set to 0.15/0.35 for small/base variants with Upernet respectively. The results and example demonstration are reported in Table 4 and Fig. 6. Compared with the standard ViT backbone, our Localformer backbone yields stable

Table 4: Semantic segmentation with Upernet 80K Xiao et al. [2018] framework on ADE20K Zhou et al. [2017]. Backbones are taken from our Localformer and the vanilla ViT pre-trained on ImageNet, respectively. “ Z_{Linear} ” means that down-up sampling of the position embedding uses Linear interpolation methods along the Zigzag index at training. The FLOPs are measured at resolution 512×512 , \dagger denotes the results are trained with Upernet 160K iterations. \ddagger means the input image size is 512×2048 . * denotes without adding deconvolution.

Backbone	Tune Res.	#Param. (M)	FLOPs (G)	mIoU (%)
ResNet-50Chen et al. [2021]	512^2	67	951 \ddagger	42.05 \dagger
DeiT-B*Chen et al. [2021]	512^2	121	2772 \ddagger	44.09 \dagger
Swin-S3-TChen et al. [2021]	512^2	60	954 \ddagger	44.87 \dagger
Swin-TLiu et al. [2021a]	512^2	60	945	44.50 \dagger
Focal-TYYang et al. [2021]	512^2	62	998 \ddagger	45.80 \dagger
StructToken-CSELin et al. [2023]	512^2	30	-	45.86 \dagger
Twins-SChu et al. [2021]	512^2	54	901 \ddagger	46.20 \dagger
ViT-S/14-336 Z_{Linear}	504^2	58	326	42.22
ViT-S/14-336Dosovitskiy et al. [2021]	504^2	58	326	44.05
Localformer-S/14-336	504^2	58	326	44.76
ViT-B/16-384 Z_{Linear}	512^2	144	395	44.28
ViT-B/16-384Dosovitskiy et al. [2021]	512^2	144	395	45.48
Localformer-B/16-384	512^2	144	395	46.34



Figure 6: Qualitative results of semantic segmentation on ADE20K Zhou et al. [2017]

gains (e.g., 0.71% mIoU on ViT-S and 0.86% mIoU on ViT-B). We also find that the performance impact of position encoding interpolation on the segmentation task is non-trivial.

Table 5: Ablation study. The effect of Hilbert token sampling and Hilbert token aggregator on the recognition accuracy for the ViT-B/16 and ViT-T/2 on ImageNet-1K and CIFAR-10 respectively.

Models	Dataset	HTS	HTA	Top-1%	Top-5%
ViT-B/16	ImageNet-1K	✗	✗	82.02	95.78
		✓	✗	82.19	95.82
		✗	✓	82.14	95.81
		✓	✓	82.47	96.00
ViT-T/2	CIFAR-10	✗	✗	83.85	99.00
		✗	✓	85.25	99.08
		✓	✗	86.32	99.15
		✓	✓	85.71	99.10

Table 6: Finetune recognition accuracy of our Localformer and ViT models on ImageNet-1K with multiple settings. And the length extrapolation validation of ViTs is reported below too. Take the original 224^2 trained model and directly test it with the scale-up inputs without tuning anything. As the length of tokens changes, we need to perform an interpolation operation on the position embedding weights. We use two interpolation methods to test the length extrapolation capability of those models.

Models	Train Res.	Tune Res.	Val. Top-1	Tune Top-1	W/o Tune		Top-1
					1D Inter.	2D Inter.	
ViT-S/14	224^2	336^2	80.10	81.99	69.89	80.50	
Ours-S/14	224^2	336^2	80.41	82.91	78.61	80.89	
ViT-B/16	224^2	384^2	81.88	83.37	66.03	81.51	
Ours-B/16	224^2	384^2	82.13	83.70	69.69	81.67	

5.3 Inspecting Localformer

Localformer is not a state-of-the-art visual model. In particular, Localformer struggles with: incorporating local information at lower layers, accurate position embedding, and good length extrapolation. To understand how the Localformer learns representations from images, we analyze its various components and the internal representation structures in this section.

Different Components To verify the effectiveness of the proposed two modules, we carry out experiments of image classification on the ImageNet-1K and a tiny CIFAR-10 datasets Krizhevsky et al. [2014]. As shown in Table 5, both HTS and HTA could achieve non-negligible gains over the original ViTs, *e.g.*, HTS gets 0.17% on ImageNet-1K and 2.47% on CIFAR-10, HTA gets 0.12% on ImageNet-1K and 1.40% on CIFAR-10. We find that the HTS and HTA are orthogonal in the image classification task, *i.e.*, their combination gets a better performance than either one of them. Specifically, the best score on the CIFAR-10 is achieved using HTS only, which indicates that Transformer-based models have over-fitting problems on a tiny dataset training from scratch.

Length Extrapolation The length extrapolation problem first appeared in the natural language processing (NLP) Press et al. [2021], it does not exist only in NLP, but also a significant issue in visual tasks Wu et al. [2021], Li and McClelland [2022]. We test the length extrapolation capability of ViT and Localformer on ImageNet-1K, in which the input number token (*e.g.*, 14×14) at training is not equal to the number token (*e.g.*, 24×24) of prediction. We also performed fine-tuning experiments with the same longer prediction tokens. During the fine-tuning phase, the weight decay, learning rate, batch size, warm-up epoch and total epoch are set to 0.1, 1e-5, 256, 10 and 30 respectively. The results are reported in Table 6, which show the advantages of the proposed Localformer (*e.g.*, 0.92% Acc on ViT-S and

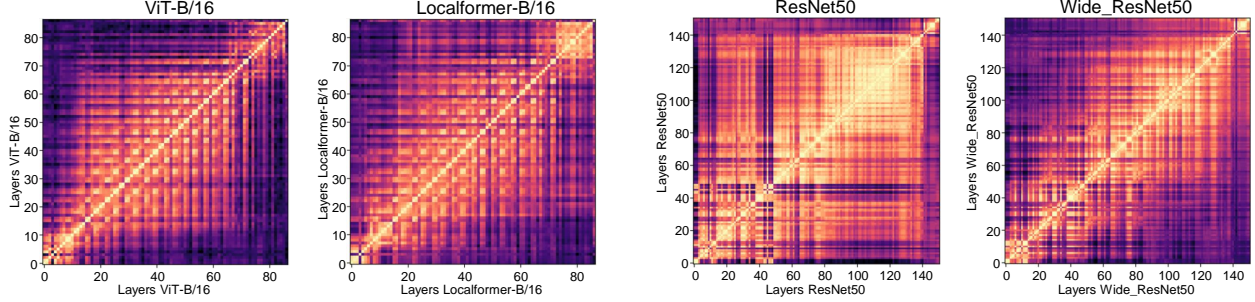


Figure 7: Representation Similarity and CKA metric. We refer to Nguyen et al. [2020], Hao et al. [2021] to calculate the CKA and report them above. The metrics are shown as heat maps, in which the x and y axes index the layers of the model. First, there are significant differences between the representational structures of ViTs and CNNs, specifically, the overall representation of ViTs is highly similar, while there is a disconnect between the shallow and deep layers of the CNNs model. We can also find that the Localformer has a relatively uniform layer similarity structure, i.e., it has a clearer grid-like pattern and a larger similarity between the shallow and deep layers.

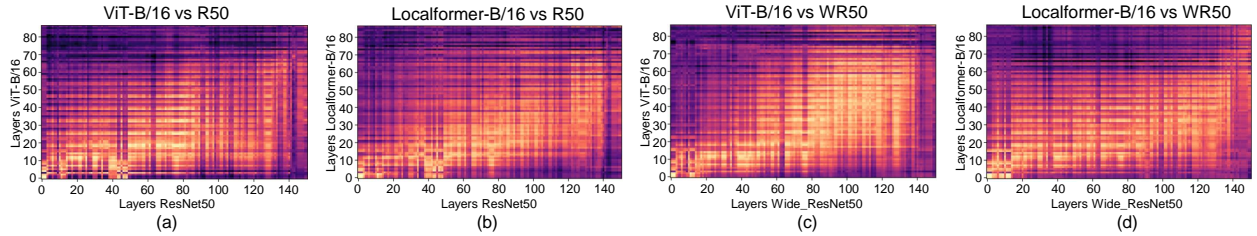


Figure 8: We also plot cross-model CKA heat maps comparing all layers of ViTs with all layers of CNNs, including the two Transformer models (i.e., ViT and our Localformer) and two CNN models (i.e., ResNet and Wide-ResNet Zagoruyko and Komodakis [2016]). (a) We find that the shallower four-fifths of ResNet layers are similar to around the shallowest half of ViT layers. The remaining one-fifth of the ResNet is similar to approximately the next third of ViT layers, with the deepest ViT layers dissimilar to shallower and deeper ResNet layers. (b) In contrast, not only the deepest one-sixth of Localformer layers is observable similar to all layers of ResNet, but also the overall representations of Localformer and ResNet are more similar. (c) We also find that the shallower third of Wide-ResNet layers are similar to around the shallowest quarter of ViT layers. The next half of Wide-ResNet layers is similar to the next half of ViT layers, with the deepest one-sixth ViT layers is somehow similar to the deeper half of Wide-ResNet layers. (d) In comparison, not only the shallower three-quarters of Localformer layers are similar to around the all layers of Wide-ResNet, but also the deepest one-sixth of Wide-ResNet layers are similar to approximately the all layers of Localformer.

0.43% Acc on ViT-B). Also, without fine-tuning, our Localformer achieves an absolute lead with the 1D interpolation method (i.e., 8.72% on ViT-S and 3.66% on ViT-B).

Representation Structure It is difficult to compare the representations of different neural networks in a meaningful way. The centered kernel alignment (CKA) Nguyen et al. [2020], Hao et al. [2021] solves this problem, which allows us to make quantitative comparisons representations of within and cross networks. The CKA has just the theoretical merits of invariance to ensure our comparative rationality, see Nguyen et al. [2020] for details. This section is to clarify whether there are represent differences between our Localformer and ViT. We plot visual representation structure for ViT and Localformer. And, we also provide the represent differences between them and the CNNs model respectively. To enable scalable comparison with our Localformer and ViT, we also refer to Raghu et al. [2021] to get the unbiased estimator of Hilbert-Schmidt independence criterion (HSIC) Song et al. [2012] using a batch of images (i.e., calculate the CKA metric on m examples). The results and analysis are reported in Fig. 7 and Fig. 8, in which our Localformer has a more uniform layer similarity structure than ViT, and its middle and shallow layers are also more similar to the CNNs model.

Position Embedding Note that our HTS and HTA do not change the parameters and calculation steps of the original position encoding module, much less a new position encoding method. To check that our method has better positional

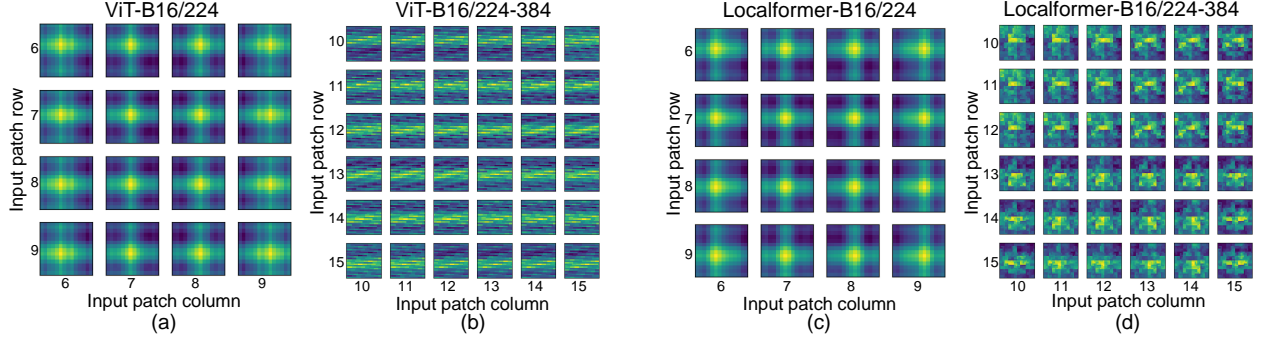


Figure 9: We refer to Dosovitskiy et al. [2021] to calculate the similarity of position embeddings for different ViTs. The brightness of a pixel indicates the cosine similarity between the position embedding of one patch with the indicated row and column and the other patches. For more clarity, we intercepted the middle patch position (i.e., 4×4 in (a) and (c), 6×6 in (b) and (d)) from all the patches (i.e., 14×14 in (a) and (c), 24×24 in (b) and (d)) for visualization. The heat maps of (b) and (d) are obtained from the original position embedding (a) and (c) by linear interpolation respectively, i.e., the operation of length extrapolation for position embedding. We find that the row-column structure shows up in (a) and (c), i.e., patches in the same row/column have similar values. The results also show that the position embedding of Localformer is more precise than it of ViT, specifically, please compare columns 6 and 9 of (a) and (c). We also find that the position encoding of ViT has lost most of its position directivity after the operation of length extrapolation, while our Localformer does not, see (b) and (d).

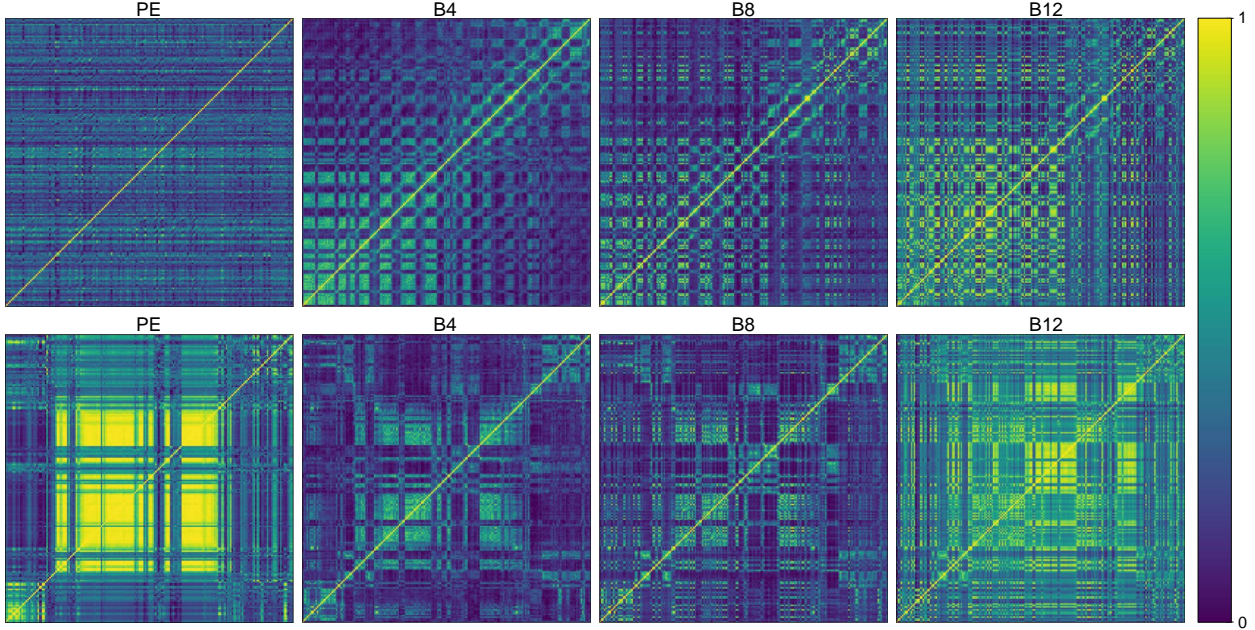


Figure 10: Token similarity and cosine distance between the patch embedding metric for the base scale ViTs (i.e., ViT-B and Localformer-B). We refer to Dosovitskiy et al. [2021] to calculate the similarity metric and report them above. The metrics are plotted as heat maps, in which the x and y axes index all the tokens of the input. For clarity, we only pick the shallower layers of patch embedding, the next Block4, Block8, and the last Block12 for demonstration. Token similarity of ViT (top) and our Localformer (bottom) show significant differences, in which the Localformer has a relatively uniform token pattern (like a self-similarity Sierpiński gasket Ida and Samborsugi [1998]) throughout the model, while the ViT suggests a much lower similarity between shallower and deeper layers. We can also find that the Localformer shows the rectangular block structure with the locality in shallow patch embedding layers, and it can provide a locality similarity between tokens at a distance, while ViT can not.

encoding capability than vanilla ViT, we refer to Dosovitskiy et al. [2021], Raghu et al. [2021] to visualize the similarity

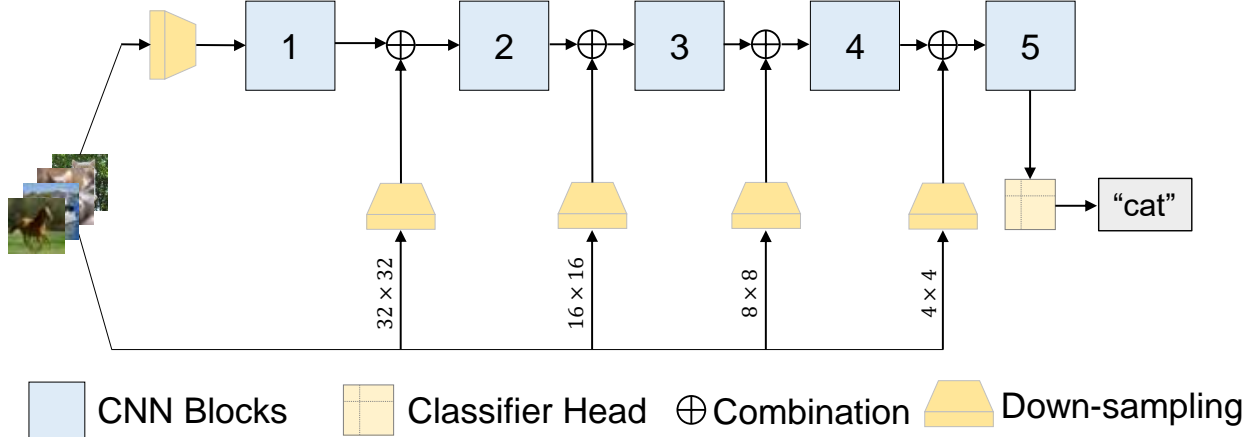


Figure 11: The illustration of the proposed FPN-MLPs network. The FPN-MLPs consist of the residual branch and a backbone network. The residual branch (below) includes an image down-sampling pyramid structure and MLPs.

of position embeddings, and the results are shown in Fig. 9. One can find that the absolute position encoding learned by our Localformer is more accurate, which may be one reason for the performance improvement achieved by the Localformer on ImageNet-1K. We also plot the new similarity of position embeddings after the linear interpolation, see Fig. 9 (b) and (d). We find that compared to the original ViT, our Localformer retains most of the position information.

Token Pattern As mentioned earlier, Localformer exhibits greater similarity across all layers and more accurate positional encoding compared to ViT. In this section, we give one sensible reason for those difference: the Localformer differs from ViT in the smoothness of the spatial information it incorporates. Are there noticeable resulting differences to the tokens of the vanilla ViT, which have fixed, token similarity in all blocks? Aim for this question, we show that the influence of patch flattening operation and a surprising connection between token similarity pattern and flattening methods. We integrate the calculation of CKA and the position embedding similarity to visualize the token similarity. The results and analysis are shown in Fig. 10, in which each heat map pixel denotes the cosine distance between a single token representation in one block and the others. One can see that the Localformer shows a more uniform token pattern in all blocks than the ViT.

Effects of HTS on MLP-only Architecture MLP-Mixer Tolstikhin et al. [2021] is a simpler all-MLP architecture than ViT. Like ViT, it also slices the input images into patches and then performs the next patch embedding operations. To verify whether our HTS is beneficial to the MLP-Mixer model, we conduct experiments on CIFAR-10 with the commonly used protocols and the data augmentation Lee et al. [2015]. As shown in Table 7, The results show that the MLP-Mixer with our HTS achieves a clear gap in the vanilla MLP-Mixer. We find this gain gap is widened under the overlapping strategy. In addition, to prove that the proposed Hilbert token sampling can enhance the stability of multi-scale representations, we employ an pyramid-structure-like MLP architecture named FPN-MLPs for the CIFAR-10 dataset, turn to Fig. 11 and Appendix Table I for details. Table 7 below presents the results, in which the FPN-MLPs using our HTS can outperform the baseline by obvious margins (i.e., 4.29%). We suppose that the HTS can provide stronger stability of multi-scale representations for the MLP-only models.

Effects of HTS on Local Window Self-attention Architecture Swin transformer adopts pyramid architectures with window self-attention to enforce the locality. In contrast to Swin, HTS elegantly exploits the locality property of space-filling curves, and it is orthogonal to the existing local window attention Transformer. We provide ablation experiments on ImageNet-1K to verify our claims. Experimental results in Table 8 show that HTS also brings gains to the advanced pyramid-based architecture.

6 Conclusion

In this paper, we propose a locality-preserving Vision Transformer named Localformer with the help of Hilbert curves. Compared with the vanilla ViT, Localformer can elegantly incorporate the local information in the shallow layers, and has a better length extrapolation. To clarify the merits of the Hilbert flattening our Localformer used, we give a comprehensive mathematical theoretical discussion and analysis in practice. Our Localformer has been validated with

Table 7: Our HTS module can be plug-and-play inserted into the MLP-based models. We conduct an ablation study on CIFAR-10 for image classification and report below. “Overlap” means that there is an overlap in ordering patches. “Pixel” means that instead of patches, pixel points are sampled. The FPN-MLP is the proposed MLP-only network with a multi-layer pyramid structure.

Models	HTS	Pixel	Overlap	Top-1%	Top-5%
Mixer-B/4	✗	✗	✗	79.73	98.34
Mixer-B/4	✓	✗	✗	80.59	98.55
Mixer-B/4	✗	✗	✓	80.48	98.32
Mixer-B/4	✓	✗	✓	81.68	98.57
Mixer-B/8	✗	✗	✗	83.58	98.71
Mixer-B/8	✓	✗	✗	84.52	98.83
FPN-MLP	✗	✓	✗	81.42	99.18
FPN-MLP	✓	✓	✗	85.71	99.58

Table 8: Our HTS module also can be inserted into the local self-attention architecture. We conduct an ablation study on ImageNet-1K for image classification and report below.

Models	HTS	Top-1%	Top-5%
Swin-S3-T Chen et al. [2021]	✗	82.08	95.63
Swin-S3-T Chen et al. [2021]	✓	82.34	95.85

better performance on image classification and semantic segmentation tasks. To better understand these results, we also examine its internal representations structure thoroughly. Future work will be aimed at how to use space-filling curves to empower the architecture design specifically for the Transformer-like networks. The code will be released upon acceptance.

References

Michael M. Bronstein, Joan Bruna, Taco Cohen, and Petar Veličković. Geometric deep learning: Grids, groups, graphs, geodesics, and gauges, 2021.

Ashish Vaswani, Noam Shazeer, Niki Parmar, Jakob Uszkoreit, Llion Jones, Aidan N Gomez, Łukasz Kaiser, and Illia Polosukhin. Attention is all you need. In *Advances in neural information processing systems*, pages 5998–6008, 2017.

Deepak Pathak, Philipp Krahenbuhl, Jeff Donahue, Trevor Darrell, and Alexei A Efros. Context encoders: Feature learning by inpainting. In *Proceedings of the IEEE conference on computer vision and pattern recognition*, pages 2536–2544, 2016.

Jian Zhang, Debin Zhao, Ruiqin Xiong, Siwei Ma, and Wen Gao. Image restoration using joint statistical modeling in a space-transform domain. *IEEE Transactions on Circuits and Systems for Video Technology*, 24(6):915–928, 2014.

Thao Nguyen, Maithra Raghu, and Simon Kornblith. Do wide and deep networks learn the same things? uncovering how neural network representations vary with width and depth. *arXiv preprint arXiv:2010.15327*, 2020.

Weixuan Sun, Zhen Qin, Hui Deng, Jianyuan Wang, Yi Zhang, Kaihao Zhang, Nick Barnes, Stan Birchfield, Lingpeng Kong, and Yiran Zhong. Vicinity vision transformer. *arXiv preprint arXiv:2206.10552*, 2022.

Andreas Steiner, Alexander Kolesnikov, Xiaohua Zhai, Ross Wightman, Jakob Uszkoreit, and Lucas Beyer. How to train your vit? data, augmentation, and regularization in vision transformers. *arXiv preprint arXiv:2106.10270*, 2021.

Chen Sun, Abhinav Shrivastava, Saurabh Singh, and Abhinav Gupta. Revisiting unreasonable effectiveness of data in deep learning era. In *Proceedings of the IEEE international conference on computer vision*, pages 843–852, 2017.

Wenhai Wang, Enze Xie, Xiang Li, Deng-Ping Fan, Kaitao Song, Ding Liang, Tong Lu, Ping Luo, and Ling Shao. Pyramid vision transformer: A versatile backbone for dense prediction without convolutions. In *ICCV*, 2021.

Ze Liu, Yutong Lin, Yue Cao, Han Hu, Yixuan Wei, Zheng Zhang, Stephen Lin, and Baining Guo. Swin transformer: Hierarchical vision transformer using shifted windows. In *Proceedings of the IEEE/CVF International Conference on Computer Vision*, pages 10012–10022, 2021a.

Kunchang Li, Yali Wang, Junhao Zhang, Peng Gao, Guanglu Song, Yu Liu, Hongsheng Li, and Yu Qiao. Uniformer: Unifying convolution and self-attention for visual recognition. *arXiv preprint arXiv:2201.09450*, 2022.

Xin Zhang and Yi Zhang. Conv-pvt: a fusion architecture of convolution and pyramid vision transformer. *International Journal of Machine Learning and Cybernetics*, pages 1–10, 2022.

Pengchuan Zhang, Xiyang Dai, Jianwei Yang, Bin Xiao, Lu Yuan, Lei Zhang, and Jianfeng Gao. Multi-scale vision longformer: A new vision transformer for high-resolution image encoding. In *Proceedings of the IEEE/CVF international conference on computer vision*, pages 2998–3008, 2021a.

Li Yuan, Yunpeng Chen, Tao Wang, Weihao Yu, Yujun Shi, Zi-Hang Jiang, Francis EH Tay, Jiashi Feng, and Shuicheng Yan. Tokens-to-token vit: Training vision transformers from scratch on imagenet. In *Proceedings of the IEEE/CVF International Conference on Computer Vision*, pages 558–567, 2021.

Ali Hassani, Steven Walton, Jiachen Li, Shen Li, and Humphrey Shi. Neighborhood attention transformer. *arXiv preprint arXiv:2204.07143*, 2022.

Daniel Bolya, Cheng-Yang Fu, Xiaoliang Dai, Peizhao Zhang, Christoph Feichtenhofer, and Judy Hoffman. Token merging: Your vit but faster. *arXiv preprint arXiv:2210.09461*, 2022.

Cedric Renggli, André Susano Pinto, Neil Houlsby, Basil Mustafa, Joan Puigcerver, and Carlos Riquelme. Learning to merge tokens in vision transformers. *arXiv preprint arXiv:2202.12015*, 2022.

Olga Russakovsky, Jia Deng, Hao Su, Jonathan Krause, Sanjeev Satheesh, Sean Ma, Zhiheng Huang, Andrej Karpathy, Aditya Khosla, Michael Bernstein, et al. Imagenet large scale visual recognition challenge. *International journal of computer vision*, 115(3):211–252, 2015.

Bongki Moon, H. V. Jagadish, Christos Faloutsos, and Joel H. Saltz. Analysis of the clustering properties of the hilbert space-filling curve. *IEEE Trans. Knowl. Data Eng.*, 13(1):124–141, 2001.

Henri Lebesgue. *Leçons sur l'intégration et la recherche des fonctions primitives*, volume 267. American Mathematical Soc., 2003.

H. V. Jagadish. Linear clustering of objects with multiple attributes. In *Proceedings of the 1990 ACM SIGMOD International Conference on Management of Data, Atlantic City, NJ, USA*, pages 332–342. ACM Press, 1990.

Craig Gotsman and Michael Lindenbaum. On the metric properties of discrete space-filling curves. *IEEE Trans. Image Process.*, 5(5):794–797, 1996.

Panagiotis Tsinganos, Bruno Cornelis, Jan Cornelis, Bart Jansen, and Athanassios Skodras. A hilbert curve based representation of semg signals for gesture recognition. In *International Conference on Systems, Signals and Image Processing, IWSSIP 2019, Osijek, Croatia, June 5-7, 2019*, pages 201–206. IEEE, 2019.

Jawadul H. Bappy, Cody Simons, Lakshmanan Nataraj, B. S. Manjunath, and Amit K. Roy-Chowdhury. Hybrid LSTM and encoder-decoder architecture for detection of image forgeries. *IEEE Trans. Image Process.*, 28(7):3286–3300, 2019.

Xueqi Zhang, Shuo Wang, Chenyu Liu, Min Zhang, Xiaohan Liu, and Haiyong Xie. Thinking in patch: Towards generalizable forgery detection with patch transformation. In *PRICAI 2021: Trends in Artificial Intelligence - 18th Pacific Rim International Conference on Artificial Intelligence*, volume 13033, pages 337–352, 2021b.

Alexey Dosovitskiy, Lucas Beyer, Alexander Kolesnikov, Dirk Weissenborn, Xiaohua Zhai, Thomas Unterthiner, Mostafa Dehghani, Matthias Minderer, Georg Heigold, Sylvain Gelly, Jakob Uszkoreit, and Neil Houlsby. An image is worth 16x16 words: Transformers for image recognition at scale. In *9th International Conference on Learning Representations, ICLR 2021, Virtual Event, Austria*, 2021.

Ze Liu, Yutong Lin, Yue Cao, Han Hu, Yixuan Wei, Zheng Zhang, Stephen Lin, and Baining Guo. Swin transformer: Hierarchical vision transformer using shifted windows. In *ICCV*, 2021b.

Ilya O. Tolstikhin, Neil Houlsby, Alexander Kolesnikov, Lucas Beyer, Xiaohua Zhai, Thomas Unterthiner, Jessica Yung, Andreas Steiner, Daniel Keysers, Jakob Uszkoreit, Mario Lucic, and Alexey Dosovitskiy. Mlp-mixer: An all-mlp architecture for vision. *CoRR*, abs/2105.01601, 2021.

Ofir Press, Noah A Smith, and Mike Lewis. Train short, test long: Attention with linear biases enables input length extrapolation. *arXiv preprint arXiv:2108.12409*, 2021.

Shun Kiyono, Sosuke Kobayashi, Jun Suzuki, and Kentaro Inui. Shape: Shifted absolute position embedding for transformers. *arXiv preprint arXiv:2109.05644*, 2021.

Jianlin Su, Yu Lu, Shengfeng Pan, Ahmed Murtadha, Bo Wen, and Yunfeng Liu. Roformer: Enhanced transformer with rotary position embedding. *arXiv preprint arXiv:2104.09864*, 2021.

Ta-Chung Chi, Ting-Han Fan, Peter J Ramadge, and Alexander Rudnicky. Kerple: Kernelized relative positional embedding for length extrapolation. *Advances in Neural Information Processing Systems*, 35:8386–8399, 2022.

Kan Wu, Houwen Peng, Minghao Chen, Jianlong Fu, and Hongyang Chao. Rethinking and improving relative position encoding for vision transformer. In *Proceedings of the IEEE/CVF International Conference on Computer Vision*, pages 10033–10041, 2021.

Hans Sagan. *Space-filling curves*. Springer Science & Business Media, 2012.

Giuseppe Peano. Sur une courbe, qui remplit toute une aire plane. *Mathematische Annalen*, 36(1):157–160, 1890.

George F Simmons. *Introduction to topology and modern analysis*, volume 44. Tokyo, 1963.

David Hilbert. Über die stetige abbildung einer linie auf ein flächenstück. In *Dritter Band: Analysis-Grundlagen der Mathematik-Physik Verschiedenes*, pages 1–2. Springer, 1935.

Jun Tian. Reversible data embedding using a difference expansion. *IEEE transactions on circuits and systems for video technology*, 13(8):890–896, 2003.

Wanli Chen, Xinge Zhu, Guojin Chen, and Bei Yu. Efficient point cloud analysis using hilbert curve. In *Computer Vision–ECCV 2022: 17th European Conference, Tel Aviv, Israel, October 23–27, 2022, Proceedings, Part II*, pages 730–747. Springer, 2022.

Konstantin Bauman. The dilation factor of the peano-hilbert curve. *Mathematical Notes*, 80:609–620, 11 2006.

Zhenyu Wang, Xuemei Xie, Qinghang Zhao, and Guangming Shi. Filter clustering for compressing cnn model with better feature diversity. *IEEE Transactions on Circuits and Systems for Video Technology*, 2022.

Donald J Berndt and James Clifford. Using dynamic time warping to find patterns in time series. In *KDD workshop*, volume 10, pages 359–370. Seattle, WA, USA:, 1994.

Huihui Fang, Jianjun Zhu, Danni Ai, Yong Huang, Yurong Jiang, Hong Song, Yongtian Wang, and Jian Yang. Greedy soft matching for vascular tracking of coronary angiographic image sequences. *IEEE Transactions on Circuits and Systems for Video Technology*, 30(5):1466–1480, 2020. doi:10.1109/TCSVT.2019.2903883.

Meinard Müller. Dynamic time warping. *Information retrieval for music and motion*, pages 69–84, 2007.

Reoxiang Li, Bing Zeng, and M.L. Liou. A new three-step search algorithm for block motion estimation. *IEEE Transactions on Circuits and Systems for Video Technology*, 4(4):438–442, 1994. doi:10.1109/76.313138.

Yin Li, Xiaodi Hou, Christof Koch, James M Rehg, and Alan L Yuille. The secrets of salient object segmentation. In *Proceedings of the IEEE conference on computer vision and pattern recognition*, pages 280–287, 2014.

Hugo Touvron, Matthieu Cord, Matthijs Douze, Francisco Massa, Alexandre Sablayrolles, and Hervé Jégou. Training data-efficient image transformers & distillation through attention. In *International Conference on Machine Learning*, pages 10347–10357. PMLR, 2021.

Minghao Chen, Kan Wu, Bolin Ni, Houwen Peng, Bei Liu, Jianlong Fu, Hongyang Chao, and Haibin Ling. Searching the search space of vision transformer. *Advances in Neural Information Processing Systems*, 34:8714–8726, 2021.

Haoqi Fan, Bo Xiong, Karttikeya Mangalam, Yanghao Li, Zhicheng Yan, Jitendra Malik, and Christoph Feichtenhofer. Multiscale vision transformers. In *Proceedings of the IEEE/CVF International Conference on Computer Vision*, pages 6824–6835, 2021.

Alec Radford, Jong Wook Kim, Chris Hallacy, Aditya Ramesh, Gabriel Goh, Sandhini Agarwal, Girish Sastry, Amanda Askell, Pamela Mishkin, Jack Clark, et al. Learning transferable visual models from natural language supervision. In *International conference on machine learning*, pages 8748–8763. PMLR, 2021.

Tete Xiao, Yingcheng Liu, Bolei Zhou, Yuning Jiang, and Jian Sun. Unified perceptual parsing for scene understanding. In *Proceedings of the European conference on computer vision (ECCV)*, pages 418–434, 2018.

Bolei Zhou, Hang Zhao, Xavier Puig, Sanja Fidler, Adela Barriuso, and Antonio Torralba. Scene parsing through ade20k dataset. In *Proceedings of the IEEE conference on computer vision and pattern recognition*, pages 633–641, 2017.

Jianwei Yang, Chunyuan Li, Pengchuan Zhang, Xiyang Dai, Bin Xiao, Lu Yuan, and Jianfeng Gao. Focal self-attention for local-global interactions in vision transformers. *arXiv preprint arXiv:2107.00641*, 2021.

Fangjian Lin, Zhanhao Liang, Sitong Wu, Junjun He, Kai Chen, and Shengwei Tian. Structtoken: Rethinking semantic segmentation with structural prior. *IEEE Transactions on Circuits and Systems for Video Technology*, 2023.

Xiangxiang Chu, Zhi Tian, Yuqing Wang, Bo Zhang, Haibing Ren, Xiaolin Wei, Huaxia Xia, and Chunhua Shen. Twins: Revisiting the design of spatial attention in vision transformers. *Advances in Neural Information Processing Systems*, 34:9355–9366, 2021.

Jia Deng, Wei Dong, Richard Socher, Li-Jia Li, Kai Li, and Li Fei-Fei. Imagenet: A large-scale hierarchical image database. In *CVPR*, pages 248–255. Ieee, 2009.

MMSegmentation Contributors. MMSegmentation: Openmmlab semantic segmentation toolbox and benchmark. <https://github.com/open-mmlab/mmsegmentation>, 2020.

Fusheng Hao, Fengxiang He, Jun Cheng, and Dacheng Tao. Global-local interplay in semantic alignment for few-shot learning. *IEEE Transactions on Circuits and Systems for Video Technology*, 32(7):4351–4363, 2021.

Sergey Zagoruyko and Nikos Komodakis. Wide residual networks. *arXiv preprint arXiv:1605.07146*, 2016.

Alex Krizhevsky, Vinod Nair, and Geoffrey Hinton. The cifar-10 dataset. *online: http://www.cs.toronto.edu/kriz/cifar.html*, 55(5), 2014.

Yuxuan Li and James L McClelland. Systematic generalization and emergent structures in transformers trained on structured tasks. *arXiv preprint arXiv:2210.00400*, 2022.

Takashi Ida and Yoko Sambonsugi. Image segmentation and contour detection using fractal coding. *IEEE transactions on circuits and systems for video technology*, 8(8):968–975, 1998.

Maithra Raghu, Thomas Unterthiner, Simon Kornblith, Chiyuan Zhang, and Alexey Dosovitskiy. Do vision transformers see like convolutional neural networks? *Advances in Neural Information Processing Systems*, 34:12116–12128, 2021.

Le Song, Alex Smola, Arthur Gretton, Justin Bedo, and Karsten Borgwardt. Feature selection via dependence maximization. *Journal of Machine Learning Research*, 13(5), 2012.

Chen-Yu Lee, Saining Xie, Patrick Gallagher, Zhengyou Zhang, and Zhuowen Tu. Deeply-supervised nets. In *Artificial intelligence and statistics*, pages 562–570. PMLR, 2015.

Jian Zhang, Sei-ichiro Kamata, and Yoshifumi Ueshige. A pseudo-hilbert scan algorithm for arbitrarily-sized rectangle region. In *International Workshop on Intelligent Computing in Pattern Analysis and Synthesis*, pages 290–299. Springer, 2006.

Lutz Tautenhahn. Draw a space-filling curve of arbitrary size. http://lutanhon.net/pic2html/draw_sfc.html, 2003.

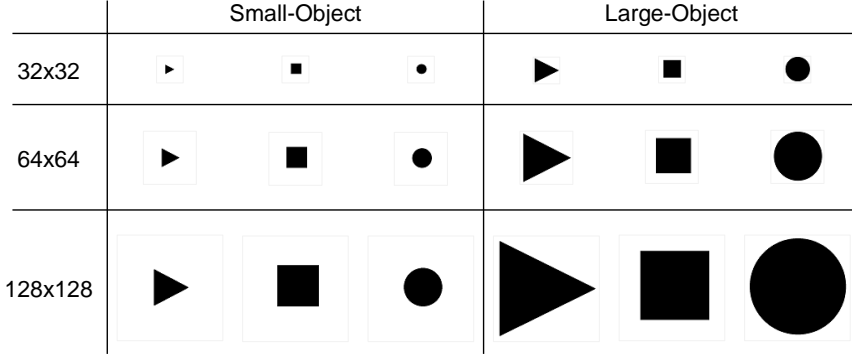


Figure 12: Three common image shapes including “circle”, “square” and “triangle” are generated. Each shape consists of three resolutions (32×32 , 64×64 , 128×128) and two object scales (i.e., large and small).

Table 9: The outline of the proposed network architecture FPN-MLPs. The output size of each block is the input size of the next one, see Fig. 11 for details. From top to bottom, the components appear in sequence. Each component may appear multiple times in FPN-MLPs.

Type	Patch size/Stride or Remarks	Input Size
Conv1D	$7 \times 1/1$	3×1024
Conv1D	$5 \times 1/2$	64×256
Conv1D	$3 \times 1/2$	256×64
Conv1D	$3 \times 1/2$	512×16
Conv1D	$3 \times 1/1$	$3 \times 1024/256/64/16$
Conv1D	$1 \times 1/1$	$3 \times 1024/256/64/16$
GELU	$3 \times 1/1$	$3 \times 1024/256/64/16$
LayerNorm	$3 \times 1/1$	$3 \times 1024/256/64/16$
AvgPool1D	16×1	512×16
Linear	<i>Logits</i>	1×512
Softmax	<i>Classifier</i>	1×10

Appendix

Additional details and results from the different sections are reported below. As shown in Fig. 12, we give the toy dataset for computing the Dynamic Time Warping Distance in Sec. 3.2. We also provide the outline of our designed MLP-only network FPN-MLPs, as reported in Table 9.

Additional Representation Structure Results As mentioned in Sec. 5.3, In this section, we provide the additional representation structure of within and cross larger models (i.e., ViT-L vs Localformer-L), and the results and analysis are shown in Fig 15. One can see that the shallow layer of our Localformer-L is significantly more similar to the middle layer of the CNNs. We also find that the Localformer-L has a more uniform layer similarity structure than ViT-L.

Additional Position Embedding Similarity Results As described in Sec. 5.3, In this section, we provide the specific and detailed similarity of position embeddings, as shown in Fig 14. We find that the Localformer has more precise position indication, while the original ViT is susceptible to horizontal or vertical position points. Additionally, when performing re-scaling on the position encoding tensor, our Localformer could keep most of the position information, while the original method loses the horizontal position information.

Generalization Capacity of Hilbert flattening Towards a simplified theoretical analysis, we focus on the grid with equal size of height and width (2^n). As shown in Fig. 13, following a simple recursive algorithm proposed in Tautenhahn [2003], Zhang et al. [2006], the general Hilbert flattening can cover grid with arbitrary size.

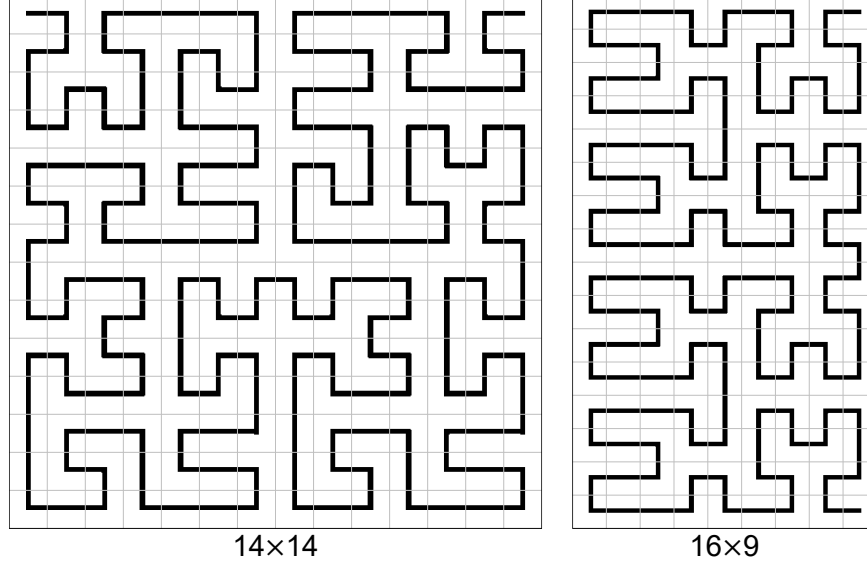


Figure 13: Thanks to Zhang et al. [2006] and Tautenhahn [2003], we show here examples of arbitrary Hilbert flattening. Left: at resolution 14×14 , Right: at resolution 16×9 .

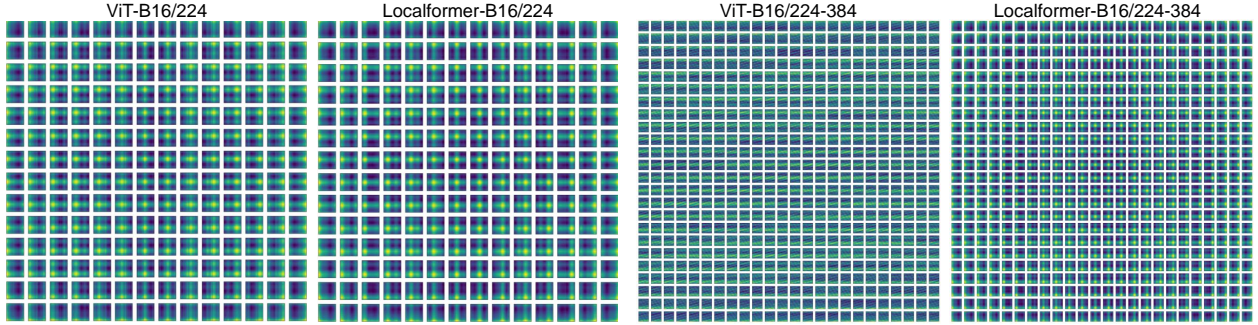


Figure 14: For clarity, same as Fig. 9, we provide all the patches of the similarity of position embeddings for different ViTs.

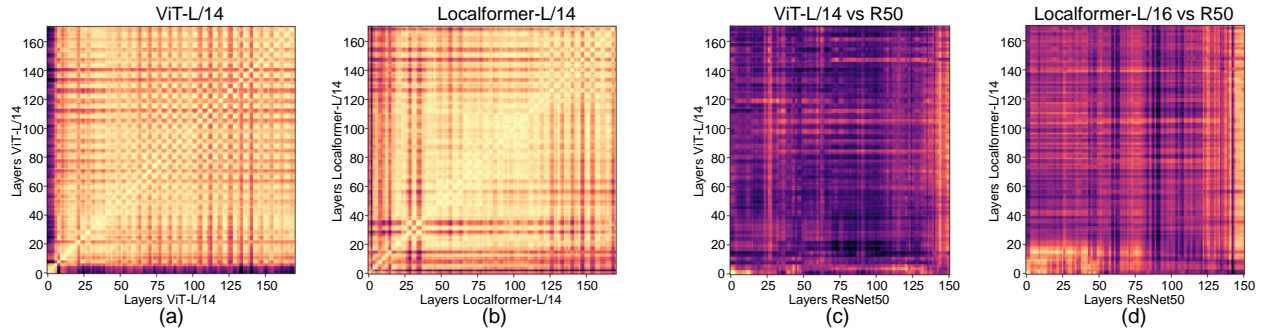


Figure 15: We give the representation similarity and CKA metric of large-scale ViTs (i.e., (a) ViT-L/14, and (b) Localformer-L/16). We find that the overall representation of Localformer-L is more similar than that of ViT-L. We also give the cross-model CKA heat maps comparing all layers of large-scale ViTs with all layers of ResNet50 (i.e., (c) ViT-L/14 vs ResNet50, and (d) Localformer-L/16 vs ResNet50). One can find that not only the shallowest layers of Localformer-L is similar to the shallower third of ResNet50 layers, but also the overall representations of Localformer-L and ResNet50 are more similar. They serve as a complement to Fig. 7 and Fig. 8.